Proton triggered emission and selective sensing of 2,4,6-trinitro phenol using a fluorescent hydrosol of 2-phenylquinoline

6.1. Introduction

Quinoline ring occurs in different natural products and represents a key motif in medicinal chemistry [303-306]. 2-Phenyl-substituted quinolines are very important quinoline derivatives associated with different biological activities such as antimalarial and antitumor agents [307] as well as efflux pump inhibitors (EPIs) [308]. The development of various competent solid organic luminophores is an escalating area, due to the potential applications of these materials in fluorescence imaging [309], organic light-emitting devices (OLEDs) [310], organic field-effect transistors (OFETs) [311,312], organic solar cells [313], chemical sensing [314], biological markers [315] etc. organic [316] and organic-inorganic hybrid [317] luminophore based chemosensors are gaining increasing attention owing to its high sensitivity, simplicity, quick response both in solution and solid phases. However, many of the developed organic fluorophores are highly emissive in solution phase but their emission in the aggregated form or in solid state is quenched due to strong π-π interactions. This phenomenon is known as aggregation-caused quenching (ACQ) effect and in some cases are attributed to the formation of species, such as exciplexes and excimers in the condensed phase [318-322]. Alternatively, chromospheres which are non- emissive in dilute solution, may become highly fluorescent in the solid state, due to restriction of their molecular motion preventing non-radiative relaxation. This phenomenon is called aggregation induced emission (AIE) effect [323,324]. There are another class of molecules which displayed very weak fluorescence in good solvent, while strong emission was observed when they were placed in poor solvent. This phenomenon is known as aggregation induced emission enhancement (AIEE) effect [325-329].

These fluorophores of AIEE characteristics not only assure great potential applications in optical sensors [330-333], electroluminescent materials [334], organic photovoltaic cells [335] and organic photoemitters [336], but also challenge the current knowledge of the photoluminescence process and extend our understanding on fluorescence mechanisms. Their mechanisms of action are usually explained in terms of, restriction of intermolecular rotation (RIR) [337], intramolecular charge-transfer (ICT) [338], intramolecular hydrogen bond [339] formation of excited-state proton transfer [340], etc. Well-designed chromophores containing strong recognizing elements showing shifts to both

absorption and emission upon acid/base stimuli are of increasing interest for their potential applications in sensors [341–346]. Great attempt has been dedicated to the molecular design and origin of the spectral shift upon protonation of functional chromophores but in maximal investigations the spectral shift in the presence of acid incentive shows a hypsochromic shift due to protonation. While lone pairs of heteroatoms lose conjugation, this hypsochromism in spectra is an obvious incident [347]. But the bathochromic shift is rare in the presence of acid stimuli.

Much effort has been devoted to synthesize organic nano/microparticles of several shapes and sizes. These include (0-D) spherical [348], (1-D) nano rods and wires [349,350], (2-D) nanoplates [351], (3-D) cubic symmetry [352], micro rods, bars, plates, panicle [353,354], and various methods were developed to prepare organic nano/microparticles, such as reprecipitation [355], self-organization [356], physical vapor deposition [357], template method [358], ultra-sonication [359], chemical reactions [360], etc. Among the above-mentioned methods, reprecipitation is one of the favoured routes towards the cost-effective large-scale production of nano/micro building blocks.

Explosives are generally polynitrated organic compounds such as Trinitrotoluene (TNT), Dinitrotoluene (DNT), and 2,4,6-Trinitrophenol /picric acid (TNP/PA). Among the different nitroaromatic compounds, TNP is one of the powerful explosives and a highly water-soluble pollutant, has recently attracted significant importance in the field of sensors pertaining to forensic investigations, as well as environmental protection, national security, human health [361-363] etc. Due to the adaptable applications of TNP in dye, matchbox industries, fireworks, drugs, glass and leather industries [364], it pollutes natural water and has acute outcome on human health, viz., cancer and damage to the kidney, liver, breathing organs [365,366] etc. Existing TNP detection systems rely on a wide range of instrument techniques [367-371] like gas chromatography-mass spectrometry (GC-MS), surface-enhanced Raman spectroscopy (SERS), ion mobility spectrometry (IMS), cyclic voltammetry, X-ray diffraction, nuclear quadrupole resonance (NQR), etc. These techniques are highly selective, but moderately complex and involve expensive instrumentation.

Recently, AIE/AIEE active materials have been used as sensors for the detection of nitroaromatics [372]. At the same time, some ICT based probes for TNP detection were reported separately by Kumar et al. [373] and Pang et al. [374]. However, most of these sensors are feasible in organic solvents, unable of detecting TNP in complete aqueous media and are based on conventional sensing mechanisms such as photo induced electron transfer (PET) [375] and formation of a ground-state electrostatic complex between electron deficient

compounds and electron rich aromatic host [376]. Also, nitrophenolic TNP being the targeted analyte, H-bond donor shred in the probe should simplify strong H-bonding interactions basically selective for TNP over its congener nitro-explosives. Yet, many are found to be costly and cumbersome. On the contrary, fluorescent based probes offer high portability, sensitivity, and real-time monitoring at low cost [377,378]. Therefore, the development of a simple and cost-effective method or a serviceable prototype for monitoring TNP in aqueous medium with high selectivity is enviable to stop rising terrorist threats as well as environmental protection due to its toxic nature. In few years ago, different types of efficient fluorescent sensors emerged for TNP. Most of the TNP sensor systems were studied in their molecular state. However, some previously reported sensors have some drawbacks which embrace low binding affinity to TNP and thrusting from other nitro compound. But the fluorescent aggregated hydrosol has this advantage over other organic sensors.

In this context, herein we report 2-phenylquinoline (**P^4**) which is weakly emissive in solution state but exhibits strong AIEE in aggregated state due to restriction of intramolecular free rotation (Scheme 1). One more attractive part of **P^4** hydrosol is its proton triggered tunable aggregation induced emission enhancement (AIEE) and intramolecular charge transfer (ICT) property. In presence of proton, an abnormal bathochromic shift is observed both in UV-Vis and FL spectra due to introduction of CT character in **P^4** upon protonation to its quinoline group. But the novelty of this work is that **P^4** exhibits strong AIEE effect, strong proton capture ability and also selective sensor activity towards TNP in aqueous medium at a concentration as low as 0.43 μM. This aggregated **P^4** hydrosol is utilized in sensing TNP which is a powerful explosive among the different nitroaromatic compounds and environmental pollutant. Detection of trace amounts of TNP and the fluorescence quenching is explained due to ground state complexation with quenching constant (Kq), 7.8 x 10^4 M^{-1}.

6.2. Experimental Section

6.2.1. Materials

2-phenylquinoline was purchased from Sigma-Aldrich Chemical Corp. Tetrahydrofuran (THF) was obtained from S. D. Fine-Chem Ltd. All the solvents used were of analytical grade. THF was distilled from sodium/benzophenone under argon atmosphere to make it free from moisture, oxygen and peroxide. Sodium dodecyl sulphate (SDS) was purchased from Merck India Ltd. and was recrystalized from 1:1 ethanol water mixture. 2,4,6 tri-nitrophenol (TNP), dinitro benzene (DNB), 4-nitrophenol (NP), 4-nitro aniline (NA), 2, 4-dinitrophenol (DNP) and 2, 4-dinitro toluene (DNT) were purchased from E-Merck India Ltd.

The purity of these chemicals was checked spectrophotometrically. Triply distilled deionized water was used throughout the experiments.

6.2.2. Synthesis of P^4 Microparticles

The microstructures of **P^4** were prepared by re-precipitation method and SDS was used as morphology directing agent. In a typical preparation, small volume of 1mM **P^4** in THF was injected into 5 mL of continuously stirred water and aqueous SDS separately at room temperature (25°C) for 5 min. Clearness of the solution gradually decreased with increasing concentration of **P^4** and a milky white color were appeared. The solutions were allowed to stand for 30 min. During the synthesis of sample-a, b, c, d, e & f in water, concentration of **P^4** (sample-a: 19.6μM, sample-b: 38.4μM, sample-c: 56.6μM, sample-d: 74μM, sample-e: 90.9μM, sample-f: 166.6μM) was varied in order to study the effect of concentration of **P^4** on aggregated structures. Similar method was used for the preparation of **P^4** microstructures in the presence of aqueous SDS and the samples are named as sample-a_1 to f_1 respectively where the concentration of SDS (3.4 mM) were kept constant.

We have checked the photostability of the AIEE active hydrosol using both UV-Vis and fluorescence spectroscopic techniques. Almost no change is observed in the UV-Vis spectra of the **P^4** hydrosol even after one month of its preparation. But in the fluorescence emission study, about 10% decrease in intensity of emission maxima (358 nm) is observed after one month of its preparation. Since fluorescence technique is more sensitive than UV-Vis, this decrease in fluorescence intensity may be due to photo degration of **P^4** hydrosol or may be due to the fluctuation of the power of the excitation source of fluorescence spectrophotometer after a month gap of its study. But over all we can say that our synthesized **P^4** hydrosol is showing excellent photostability.

6.2.3. pH study

During pH variation study, the pH of the medium was adjusted by adding different amounts of 0.1 M HCl and 0.1 M NaOH and the subsequent measurement of pH was done by using a pH meter. All the solutions were prepared on the same day to study their absorbance, steady-state and time-resolved fluorescence measurements.

6.2.4. Fluorescence Quantum yield study

Fluorescence quantum yield of **P^4** hydrosol (99.9% water) was determined using optically matching aqueous solutions of tryptophan (Φ_t=0.13, λ_{ex}=280 nm) as standard. The quantum yield is calculated using the following equation:

$$\Phi = \Phi_r \left(\frac{A_r F_s}{A_s F_r}\right) \frac{\eta_s^2}{\eta_r^2}$$

Where A_s and A_r are the absorbance of the sample as reference solutions respectively at the same excitation wave length, F_s and F_r are the corresponding relative integrated fluorescence intensities. η_s and η_r are the refractive index of the sample and reference solution, Φr quantum yield of the reference.

6.2.5. Characterization

UV-Vis spectroscopic measurements were carried out in a 1cm quartz cuvette with a Shimadzu UV-1800 spectrophotometer. Fluorescence spectra were recorded using Hitachi F-7000 Fluorescence Spectrophotometer. The Morphologies of the synthesized nano/microstructures were studied using a ZEISS EVO 18 Scanning Electron Microscope (SEM) with an accelerating voltage of 5 kV. Samples for the SEM study were prepared by placing a drop of the aqueous suspension of particles on a small glass slide followed by solvent evaporation under vacuum. To minimize sample charging, the dried samples were coated with a thin gold layer right before SEM study. Fluorescence lifetimes were obtained by the method of Time Correlated Single-Photon Counting (TCSPC) on a FluoroCube- 01-NL spectrometer (Horiba Jobin Yvon) using a laser-diode with the detection wavelength at 346 nm for **P[4]** hydrosol both in presence and absence of TNP. Excitation wavelength was 291 nm for all the samples. Lamp profiles were measured with a band-pass of 3 nm using Ludox as scatterer. The decay parameters were recovered using non-linear iterative fitting procedure based on the Marquardt algorithm [379]. The quality of fit was assessed over the entire decay, including the rising edge, and tested with a plot of weighted residuals and other statistical parameters e.g. the reduced $\chi 2$ ratio [380]. The signal was detected at magic angle (54.7°) polarization using a Hamamatsu MCP PMT (3809U). Time resolution of the experimental setup was ~90 ps. Optical microscopy images were taken using an NIKON ECLIPSE LV100POL upright microscope equipped with CCD camera (model no. Nikon DS-Fi l), polarizer-analyzer assembly and 100W mercury lamp as excitation source for emission study. The samples for optical microscopic study were prepared by placing a drop of the as prepared hydrosol onto a clean glass slide.

6.2.6. Detection Limit

The limit of detection (LOD) was calculated on the basis of the fluorescence titration. The fluorescence emission spectrum of **P[4]** as a function of its increasing concentration was measured five times, and the standard deviation (σ) of the blank measurement was calculated.

To obtain the slope (k), the fluorescence emission intensity at 346 nm was plotted against the increasing concentration of quencher i.e, TNP in the present study. The LOD was calculated using the following equation [381].

$$LOD = 3\ \sigma/k$$

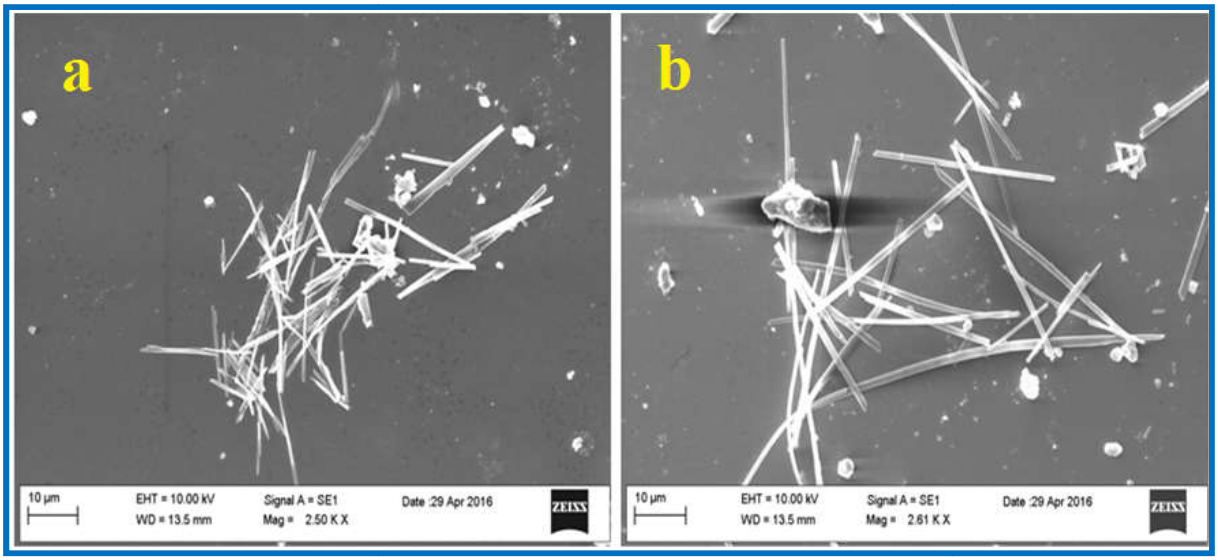

Fig. 6.1: SEM images of particles prepared in presence of 4mM SDS (a) sample-a_1, (b) sample-f_1.

6.3. Results and Discussion

6.3.1. SEM study

No regular morphology of the particles was observed when the synthesis was carried out in the absence of SDS. Scanning electron microspic (SEM) images of $\mathbf{P^4}$ microstructures with increasing concentration of phenyl quinoline ($\mathbf{P^4}$) for a fixed SDS concentration (4 mM) are shown as sample-a_1 & f_1 in ***Fig. 6.1.*** Morphology of the particles have rod like shaped at lower concentration of $\mathbf{P^4}$ and there is a clear indication that the particles grow in one dimension with the increasing concentration of $\mathbf{P^4}$.

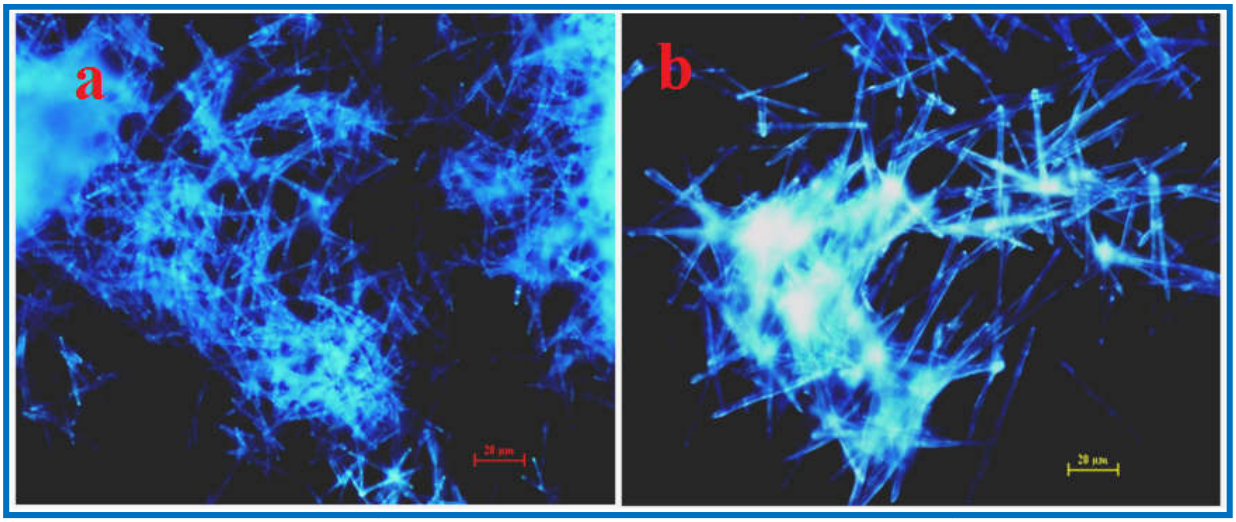

Fig. 6.2: Optical fluorescence microscopy images under UV excitation of particles prepared in presence of 4mM SDS (a) sample-a_1, (b) sample-f_1.

6.3.2. Optical microscopic study

Morphologies of the particles were observed by fluorescence microscopy are shown in ***Fig. 6.2.*** At lower concentration of phenyl quinoline (**P**^{4}) rod shaped morphology is clearly observed for the sample-a_1 & f_1 using optical microscopy. Upon UV excitation, **P**^{4} shows rod-shaped microstructures with sky blue emission. There is a clear indication that dimension of the particles increases along its length with increasing concentration of **P**^{4}. Glittering light emissions are observed at the ends of the microcrystals indicating that an optical waveguide effect is operating in the light transmission process within the microcrystals.

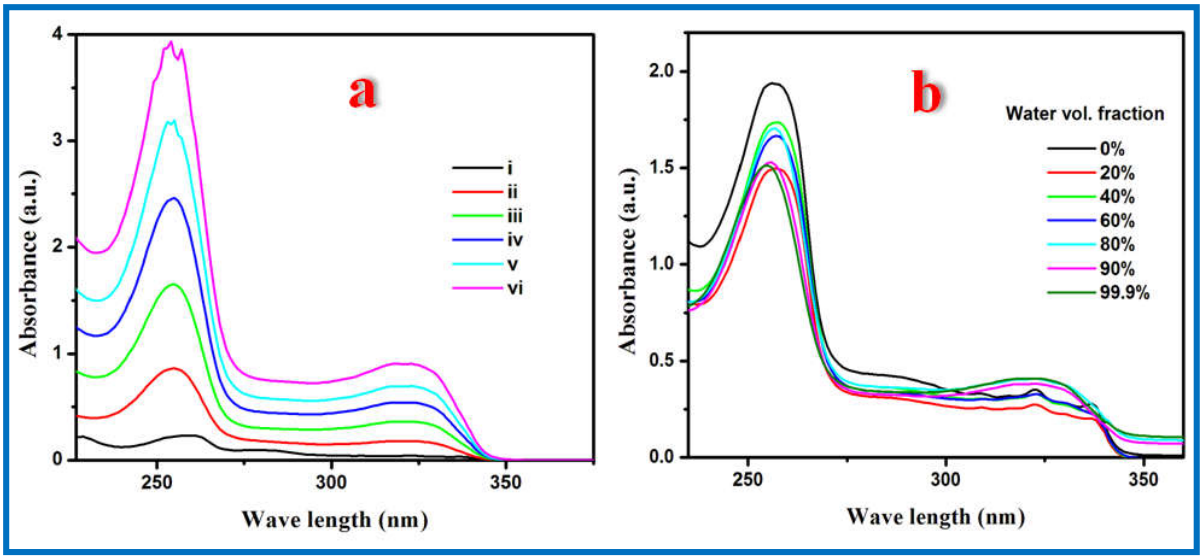

Fig. 6.3: (a)The UV-Vis absorption spectra of (i) **P**^{4} in THF (ii) sample-a, (iii) sample-b, (iv) sample-c, (v) sample-d, (vi) sample-e, (vii) sample-f, (b) UV–Vis absorption spectra of **P**^{4} in (i) 0% water (**P**^{4} in THF), (ii) 20%water, (iii) 40% water, (iv) 80% water, (v) 90% water and (vi) 99.9% water.

6.3.3. UV-Vis Study

UV-Vis absorption spectra of the compound **P**^{4} were investigated both in solution and in the aggregated state. UV–Vis absorption spectrum of **P**^{4} in THF is shown in ***Fig. 6.3a.*** and the two groups of bands are detected at 284-348 nm and 233-280 nm respectively. The first intense band with peak at ~ 255 nm is due to π- π* transition of **P**^{4}. The second broad band which is almost absent in THF, but increases with the increasing concentration of **P**^{4} in the hydrosol is due to charge transfer transition from phenyl to quinoline moieties for the more favoured planar conformation of **P**^{4} within the aggregates. The increasing intensity of the absorption band with the increasing concentration of **P**^{4} in the hydrosol has been explained due to the increased number of the charge transfer excitonic state within the aggregates. The

UV-Vis absorption spectra of the hydrosol for a fixed $\mathbf{P^4}$ concentration and increasing volume percentage of water are shown in ***Fig. 6.3b.*** It is observed that the absorption intensity of the hydrosol increases with increasing volume percentage of water in the solvent mixture. As the volume of water is increased from 0% to 60%, the absorption spectra remain unchanged. Interestingly, a sharp change of broad absorption spectra ~ 300- 340 nm region with increased intensity is observed as the volume percentage of water changes from 60% to 80%. At > 60% water fraction, the absorption spectrum is purely appeared from the aggregated hydrosol of $\mathbf{P^4}$. In addition, the overall shift of the spectral baseline at > 60% water volume fraction relative to that of the monomer is ascribed to the scattering of light by the larger aggregated structures in solution.

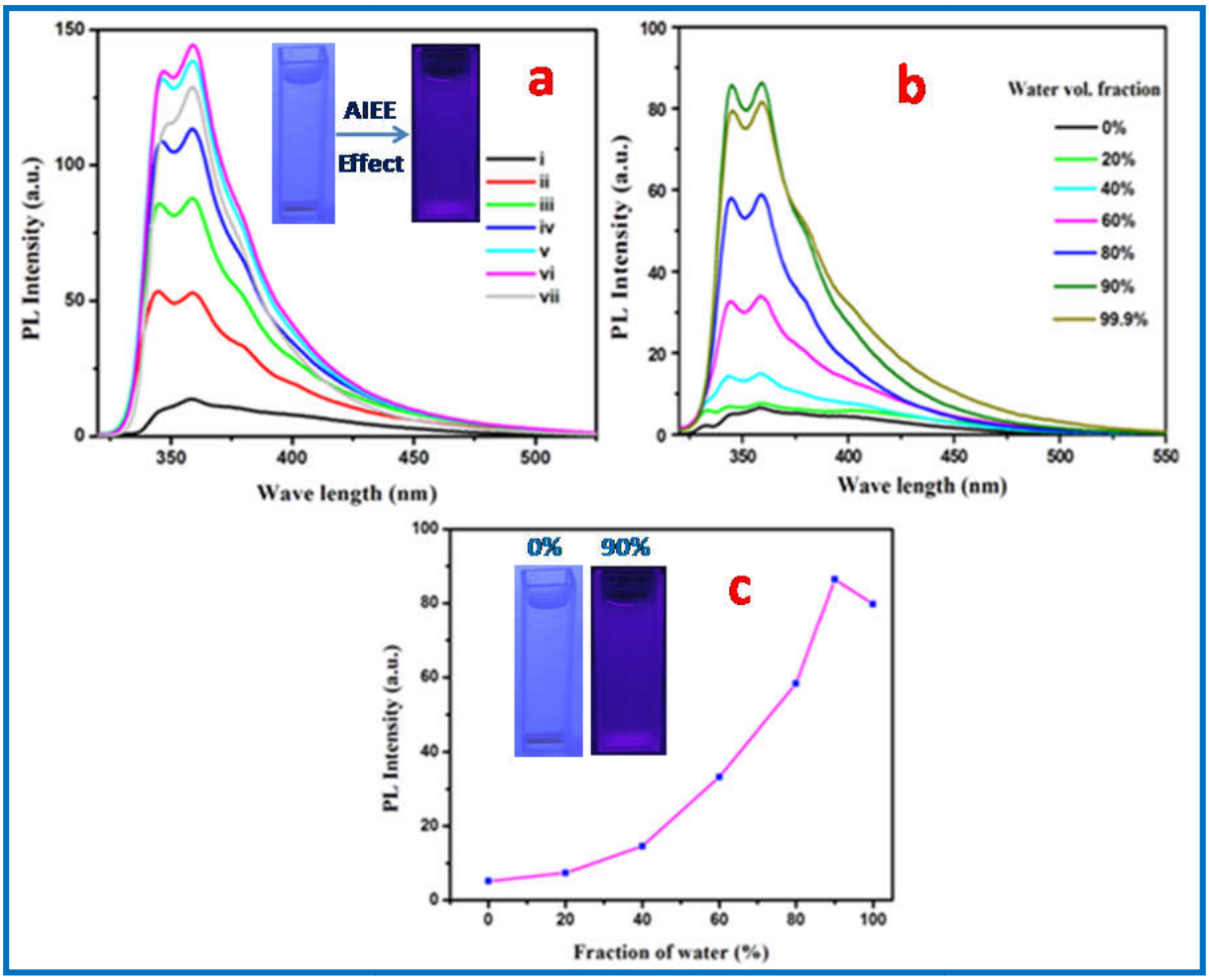

Fig. 6.4: (a)The Fluorescence emission spectra of (i) $\mathbf{P^4}$ in THF (ii) sample-a, (iii) sample-b, (iv) sample-c, (v) sample-d, (vi) sample-e, (vii) sample-f, λex: 315 nm. Inset Fluorescence images of $\mathbf{P^4}$ ($\mathbf{P^4}$ in THF and aggregated hydrosol) under 365 nm UV light illumination. (b) Emission spectra of freshly prepared $\mathbf{P^4}$ (62 μM) in 0% -99.9% water. λex: 315 nm. c) Plot of relative variation of PL intensity Vs. Volm percentage of water in the THF/water mixture. Insets: Fluorescence images of $\mathbf{P^4}$ (0% and 90% H_2O) under 365 nm illuminations.

6.3.4. Emission Study

The most important way to test the AIEE activity of a compound is to make an assessment of the emission spectra between its molecular and aggregated states. PL spectra of **P^4** in THF and its aggregated hydrosol with different amount of **P^4** are shown in ***Fig. 6.4a***. Dilute solution of **P^4** in THF (8 μM) exhibits very weak structured emission with peaks at 346, 359 and 375 nm respectively upon photoexcitation at 315 nm. But the aggregated hydrosol of **P^4** exhibits intense structured emission bands centered at 346 and 359 nm. It has been observed that the PL intensity of **P^4** hydrosol increases gradually with increasing concentration of **P^4**. This is due to aggregation induced emission enhancement (AIEE) effect and it reaches a maximum at 90.9 μM **P^4** and then decreases with a further increase in **P^4** concentration (***Fig. 6.4a***). Thus 90.9 μM is the optimum concentration of **P^4** for the AIEE, below which it forms emissive crystalline structures but further increase (> 90.9 μM) in concentration, **P^4** orients in a random fashion to soften the microcrystals and is liable for diminishing the emission intensity of the hydrosol. Emission quantum yield of **P^4** hydrosol at 99.9% vol percentage water is ~ ca 0.06 using tryptophan in water as standard. Images of solutions containing **P^4** in THF and **P^4** hydrosol (99% vol. of water) under UV irradiation are shown in the inset of ***Fig. 6.4a***.

Fig. 6.4b shows the fluorescence emission spectra of **P^4** at different volume fractions of water for a fixed concentration of **P^4** (62 μM). It is observed that the fluorescence of **P^4** is gradually intensified when water is increasingly added into its THF solution. PL intensity increases gradually up to 90% water fraction, signifying the fabulous AIEE properties of **P^4**. Restriction of the intramolecular rotations (RIR) and large amplitude vibrations (RIV) of the phenyl groups of **P^4** in the aggregated state prevent the non radiative decay routes and make the molecule a strong emitter (***Scheme 6.1***). It is also observed that PL intensity of **P^4** hydrosol decrease when the water fraction is increased from 90% to 99.9% (***Fig. 6.4b***). This is due to the formation of amorphous agglomerates. At low water content, **P^4** molecules gradually accumulate in an ordered fashion to form crystalline aggregates. But at higher water content (>90%) **P^4** may rapidly agglomerate in a random fashion to soften the microcrystals. Change of emission colour from colourless to intense sky blue in presence of 0% and 90% water content under UV light illumination are shown in the inset of ***Fig. 6.4c***.

6.3.5. Fluorescence anisotropy study

Aggregation phenomena were investigated by fluorescence anisotropy study of the **P^4** hydrosol. It is quite surprising to find that **P^4** in THF exhibits a very small average anisotropy

value ~0.03 owing to rapid rotation of the fluorophore on its lifetime scale; whereas in **P**[4] hydrosol, the average anisotropy value is increased to ~0.17 (***Fig. 6.5***).

Scheme 6.1: Proposed Mechanistic Pathway for Aggregation Induced Emission Enhancement Behavior of (**P**[4]).

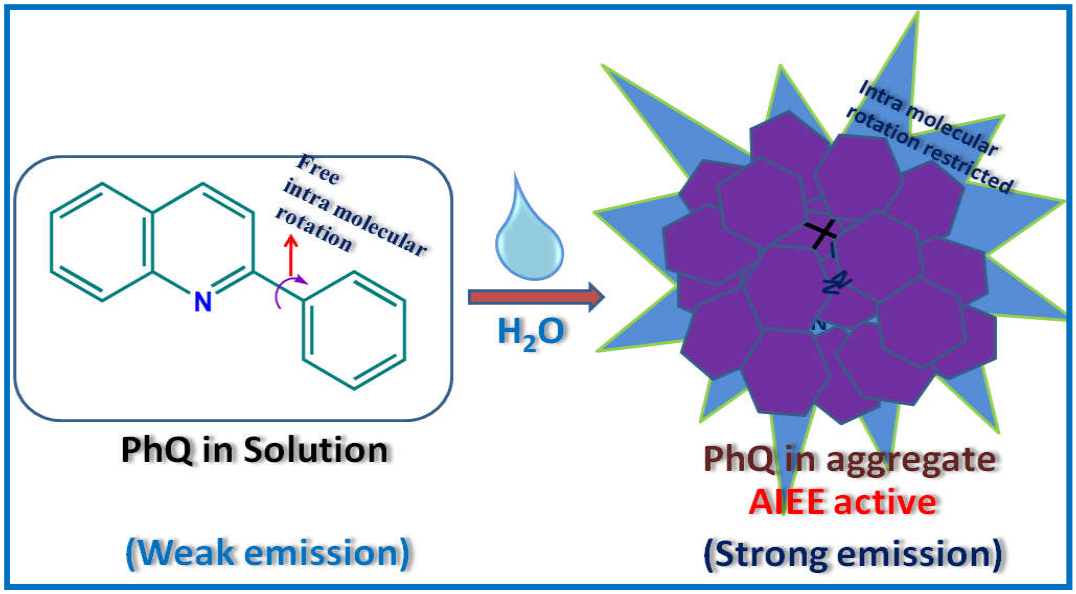

The significant increase of the anisotropy value indicates that free **P**[4] is aggregated onto large particles, and this resulted the reduction of the rotational diffusion rate [382]. In aggregates, fluorescence intensity was significantly increased due to decreasing micro environmental polarity of the ICT characteristic of quinoline chromophore.

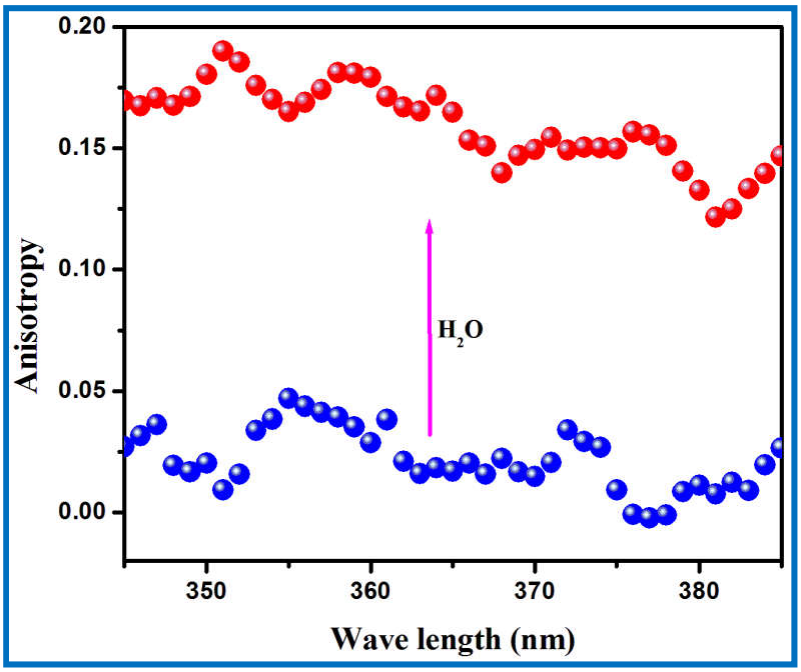

Fig. 6.5: Fluorescence anisotropy of **P**[4] in the absence and presence H_2O (9:1, v/v) solution [**P**[4] in THF] = 8 μM, [sample-e] = 90 μM, λ_{ex} = 315 nm.

6.3.6. pH dependent photophysical study

Amusingly, PL property of **P⁴** is sensitive towards acid and base. With increasing proton concentration **P⁴** get protonated at the nitrogen atom of imidazole moiety (***Scheme 6.2***). Subsequently the fluorescence colour of the solution changes considerably and visible through the naked eye after UV light illumination.

Scheme 6.2: The proposed mechanism of **P⁴** for sensing H^+

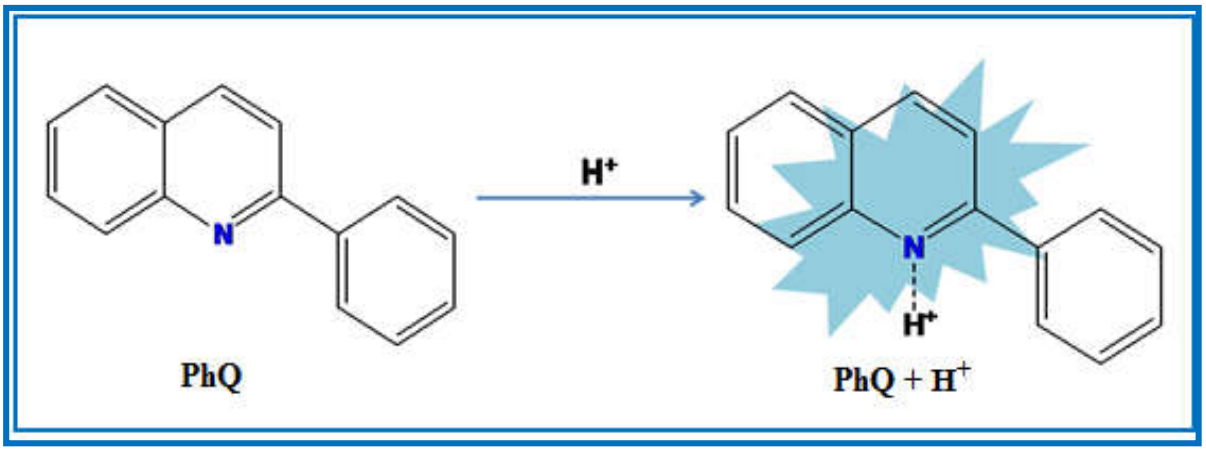

6.3.7. Absorption spectra of P⁴ at different pH

The UV-vis absorption spectra of **P⁴** hydrosol recorded at different pH values are shown in ***Fig. 6.6a***. In the acidic pH protonated form of **P⁴** shows three absorption bands peak at 340, 268, 239 nm. Absorption spectra of the deprotonated forms show two absorption band with maximum at 255nm in the basic (pH >7) medium. At higher pH >7 (basic medium) absorption spectrum is similar to that of aggregated hydrosol in water. The UV-vis absorption spectra of aggregated hydrosol of **P⁴** shows that the 255 nm band is split into two new band and the red shifted band at ~ 340 nm increases gradually with increasing H^+ ion concentration in the hydrosol. The broadening and red shift of the absorption spectra at pH <5 suggest the enhancement of charge transfer character in **P⁴** upon protonation [383].

6.3.8. Fluorescence emission of P⁴ at different pH

The PL spectra of **P⁴** hydrosol at different pH values are shown in ***Fig. 6.6b***. No significant change in the PL spectra of the hydrosol is observed at pH ≥ 6. But at pH< 6, a new ~ 50 nm red shifted broad emission band appeared having maxima at 397 nm. It is also observed that the milky hydrosol gradually turned into clear solution with increasing H^+ concentration in the medium (***Fig. 6.7***). We assume that the red shifted broad emission band at 397 nm is due to the charge transfer emission from the dissolved Protonated **P⁴** H^+ in the solution.

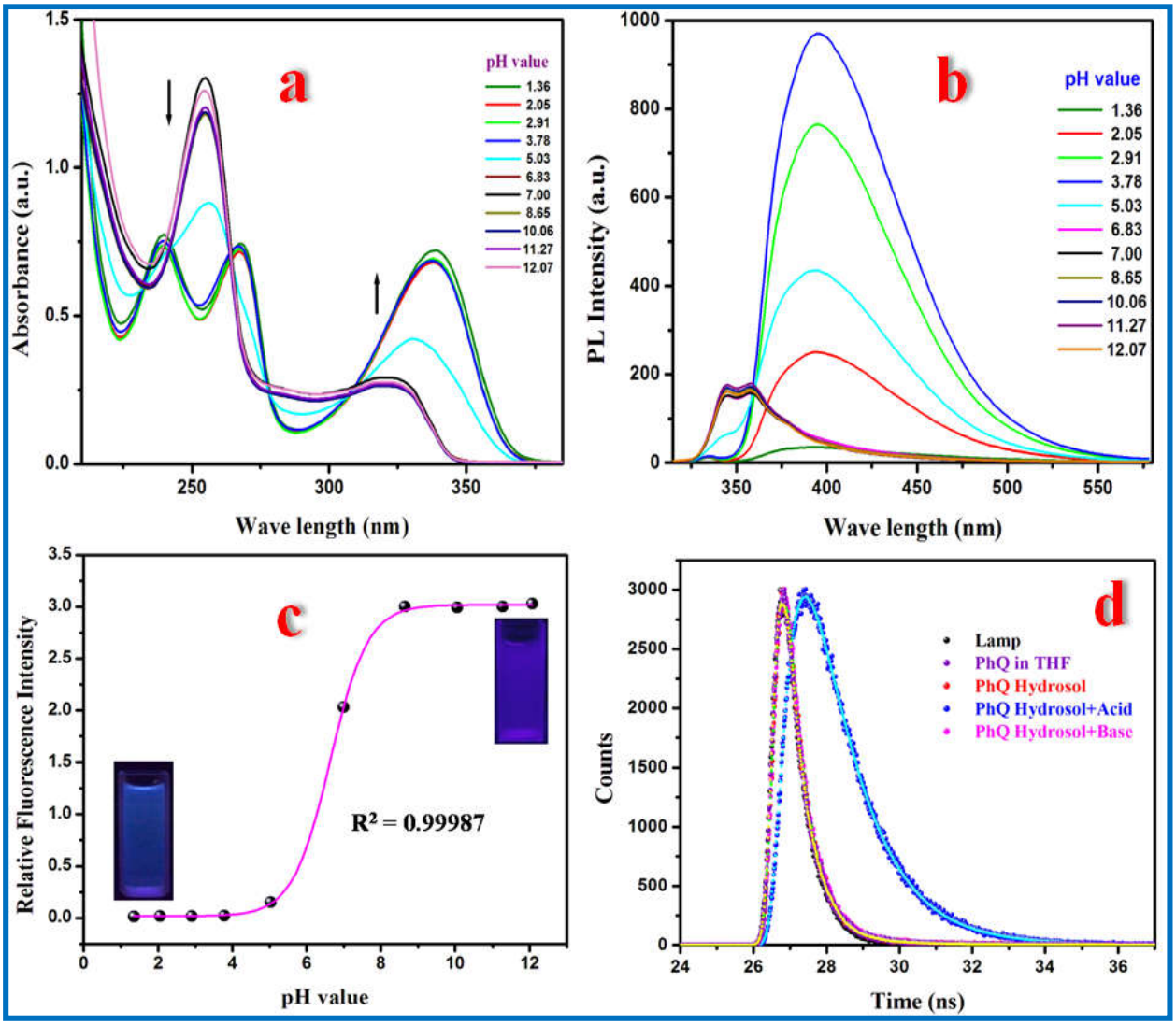

Fig. 6.6: (a) UV-Vis absorption spectra of **P**^{4} hydrosol (38.4μM) in the THF/water mixture (10 : 90 v/v) at different pH values of the medium (pH ~ 1.0–12.0). (b) PL spectra of **P**^{4} hydrosol (38.4 μM) in the THF/water mixture (10: 90 v/v) at different pH values of the medium (pH ~ 1.0–12.0). λex: 300 nm. (c) Ratiometric calibration curve of I_{345}/I_{397} (ratio of fluorescence intensity at 345 nm to that of at 397 nm) as a function of pH of the medium and pH dependent color shift from blue to sky with decreasing concentration of H+ ions in the medium under 366 nm illumination. (d) Time resolved fluorescence decay curve of **P**^{4} hydrosol (90 μM **P**^{4}) in presence of acid medium (pH ~ 4) at (λem: 397 nm) and basic medium (pH ~ 10). λem =346 nm; All spectra are taken using λem = 291 nm.

Fig. 6.6c, shows a visual change in color from blue to sky blue under UV light illumination at higher pH (> 4, blue) and lower pH (< 6, sky blue) are observed indicating the presence of mainly charge transfer protonated **P**^{4} in acidic solution. It is also observed that the intensity of the 397 nm band decreases at higher H^+ ion concentrations (pH < 4). It appears that at higher H^+ ion concentration, the electron rich nitrogen centre of the quinoline unit gets protonated and hence the charge transfer character of the molecule as a whole decreases.

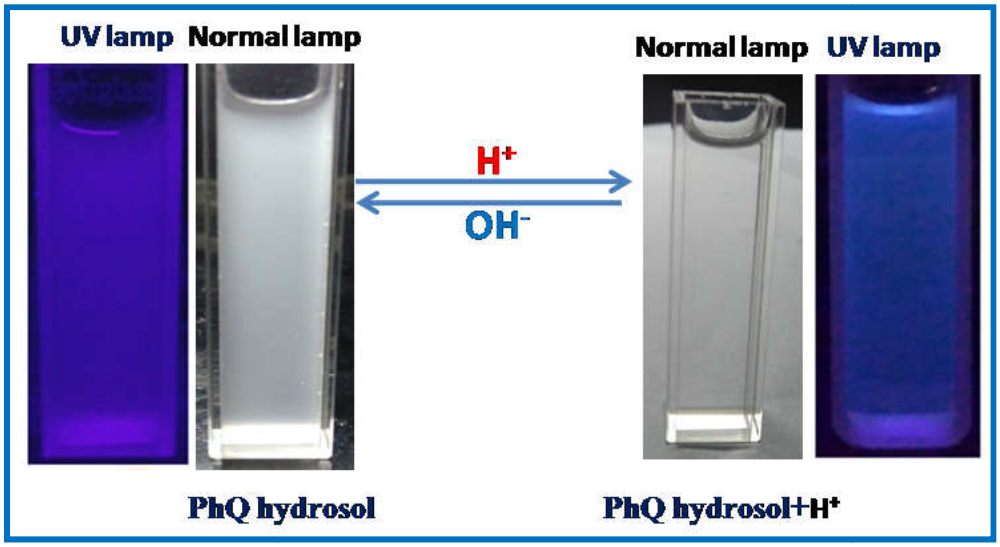

Fig. 6.7: Photographic picture of P^4 and protonated P^4 hydrosol under normal light and UV light (365 nm) irradiation.

6.3.9. Time resolved fluorescence studies

In order to better understand the mechanism of ratiometric emission behavior of the P^4 luminogen in acidic medium, time resolved emission study of P^4 hydrosols both in neutral and acidic medium was carried out with excitation at 291 nm. The decay profiles of deprotonated and Protonated hydrosols of P^4 are shown in ***Fig. 6.6d***. Fluorescence decay profile of P^4 in THF is fitted with single exponential decay and it is found to be 39 ps. Fluorescence decay profiles of P^4 hydrosols (sample- e) having rationally higher emission intensity at 346 nm in neutral medium (pH=7) is fitted with single-exponential decay. The measured emission lifetime is ~ 42 ps.

In order to understand the mechanism of ratiometric emission changes of P^4 hydrosol in presence of acidic medium, time resolved emission study at 397 nm are carried out. Time resolved emission data at 397 nm in acidic medium (pH=4) are fitted with single-exponential decay and the measured emission lifetimes is 1.21 ns. This increasing life time value 1.21 ns component arises solely from the solvated P^4H^+ upon excitation to its ICT state (***Fig. 6.6d***). We have also carried out time resolved fluorescence lifetime of P^4 hydrosol in basic medium (pH=10). Time resolved emission data at 346 nm are fitted with single exponential decay and value is ~ 35 ps. At higher pH >7 (basic medium) lifetime value is similar to that of aggregated P^4 hydrosol in water.

6.3.10. Reversibility studies

We also investigated the reversibility of protonation/deprotonation processes of P^4 in its hydrosol. In UV-Vis study, P^4 hydrosol in neutral medium shows two bands at ~320 nm and ~255 nm respectively.

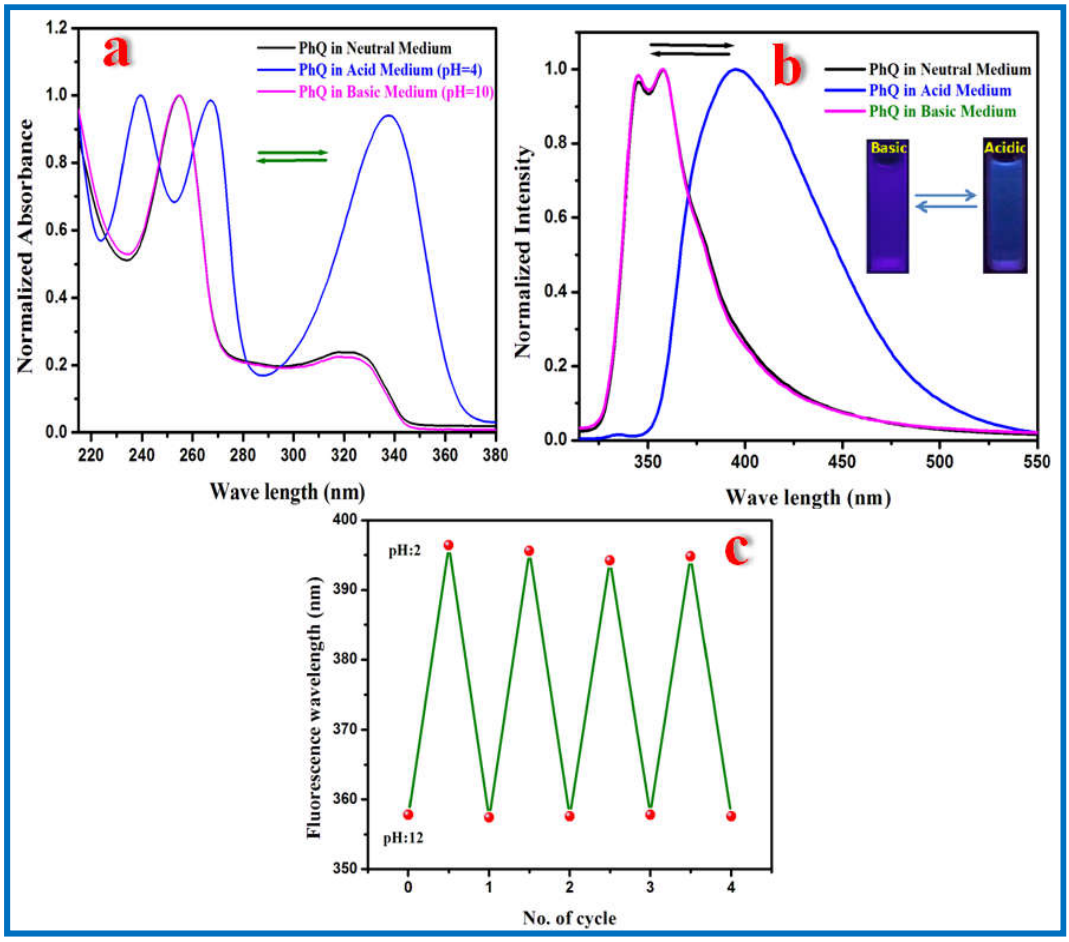

Fig. 6.8: (a) Normalized UV-Vis spectra and (b) Normalized PL spectra of aggregated $\mathbf{P^4}$ by changing the pH of the medium from basic to acidic. (c) Reversible switching of the emission wavelength of $\mathbf{P^4}$ by repeated addition of acid and alkali to the medium.

On the other hand $\mathbf{P^4}$ hydrosol in acidic medium shows ~ 20 nm red shifted broad band around at 340 nm and the 255 nm band is split into two bands. Interestingly, $\mathbf{P^4}$ hydrosol in basic medium shows similar absorption spectra as that of $\mathbf{P^4}$ hydrosol in neutral medium. This observation illustrates the reversibility character of $\mathbf{P^4}$ hydrosol in both acidic and basic medium. It is also observed that the switch between sky blue and deep blue emission can be repeated without exhaustion by swap addition of NaOH and HCl and the process is non-destructive in nature (***Fig. 6.8a***). The red shift of ~ 50 nm in the fluorescence of $\mathbf{P^4}$ hydrosol when in contact with HCl and the revival toward the initial sky blue emission (λem = 346 nm) in presence of alkali NaOH exhibit the important fluorescence switching properties of the $\mathbf{P^4}$ hydrosol under protonation/ deprotonation incentive (***Fig. 6.8b***). Reversibility of proton sensing of $\mathbf{P^4}$ hydrosol is deliberated by changing the pH of the medium from pH = 2 to pH = 12. The turn on and off ~ 397 nm band is observed as the pH of the medium changes from pH = 2 to pH = 12 and vice versa (***Fig. 6.8c***).

6.3.11. DFT Study

In order to better understand the Photophysical property as well as charger transfer character of **P**^{4}, DFT based computational study has been carried out. The frontier molecular orbital (FMO) of **P**^{4} and **P**^{4}H$^+$ calculated using the DFT/B3LYP/ 6-31G (d, p) level of theory is shown in ***Fig. 6.9***. It was well recognized that the spatial conformation of molecules played a vital role in ascertaining their stacking modes and thus affect the properties of the resulting aggregate. In the **P**^{4} one phenyl group is attached to the 2 positions of the quinoline moiety through a single bond. The free rotation of phenyl group is accountable to open up the non-radiative deactivation channels for excited **P**^{4} in its isolated form in solution. But the aggregation of **P**^{4} within the hydrosol restricts the free rotation around its single bond and makes it AIEE active. This restricted intra-molecular rotation (RIR) is the main reason of AIEE effect of **P**^{4}.

Ground state Optimized geometry of **P**^{4} using DFT/B3LYP/ 6-31G(d, p) level of theory shows that the phenyl units prefer to remain ~ 20° out of plane of the quinoline ring. HOMO electron densities of **P**^{4} are localized within the phenyl and quinoline moieties separately and the electron densities are shifted from the phenyl to the quinoline moiety in its LUMO. The highest Occupied molecular orbital (HOMO) and the lowest unoccupied molecular orbital (LUMO) energy of **P**^{4} are shown in ***Fig. 6.9*** and also calculated HOMO and LUMO energy gap and dipole moment are found to be 4.46 eV and 1.015 D respectively.

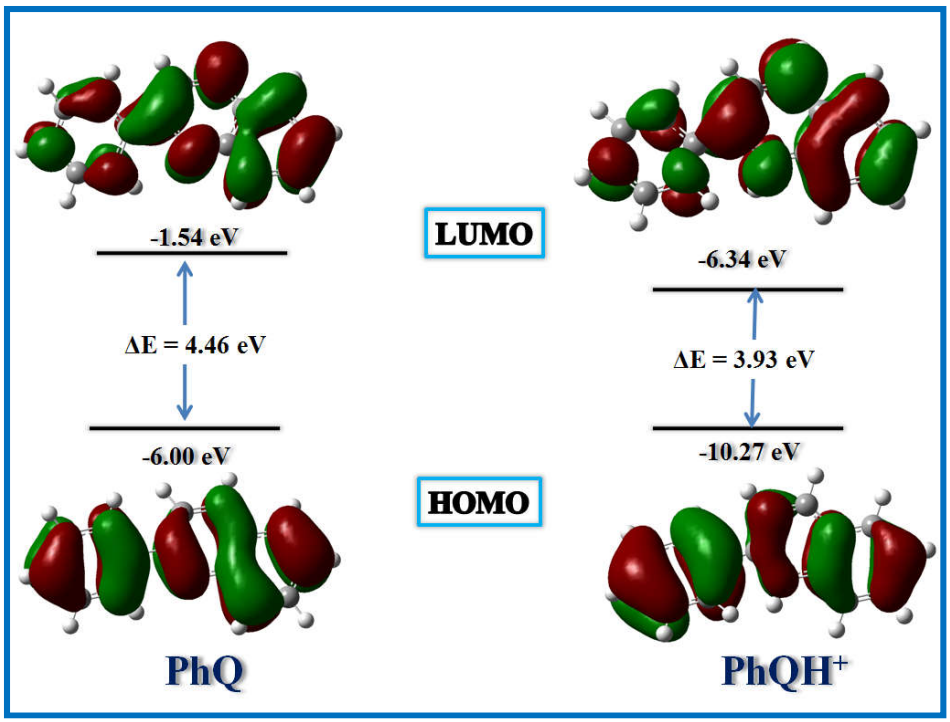

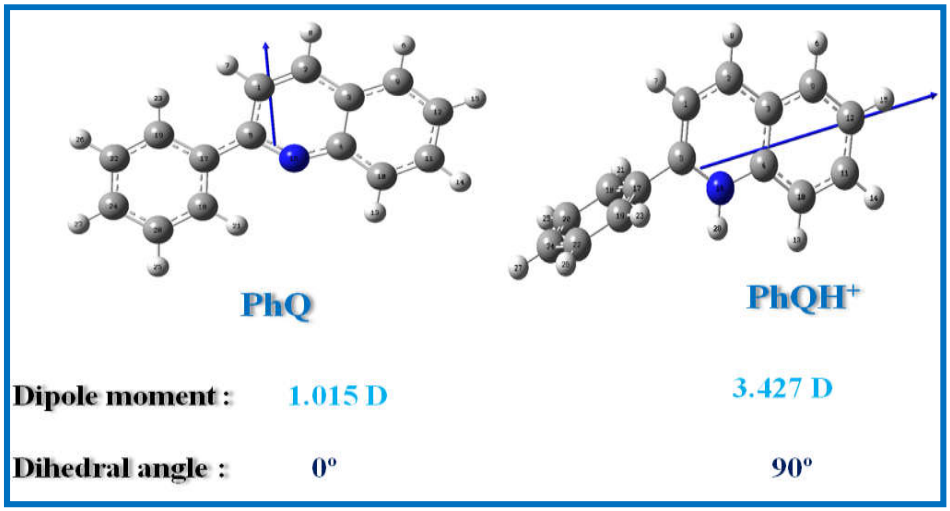

Fig. 6.9: Theoretically calculated frontier orbital of $\mathbf{P^4}$ and $\mathbf{P^4}H^+$ using the DFT B3LYP/6-31G (d, p) level of theory. The optimized geometry, dipole moment and dihedral angle of $\mathbf{P^4}$ and $\mathbf{P^4}H^+$ molecules are calculated using the TDDFT B3LYP/6-31G (d, p) level of theory.

On the other hand, Optimized Ground state geometry of $\mathbf{P^4}H^+$ using the DFT/B3LYP/ 6-31G(d, p) level of theory shows that the phenyl units prefer to remain ~ 33° out of plane of the quinoline ring. In acidic medium, the proton (H^+) will attach with the nitrogen atom of the quinoline groups. Through aromatic conjugation, electron density is shifted from phenyl group to the quinoline group in its LUMO. Thus a swept ICT character from the donor phenyl to the acceptor protonated quinoline group takes place and is reflected in the lowering of HOMO and LUMO energy gaps from 4.46 eV to 3.93 eV after protonation. It causes a red-shift of both the absorption and emission spectra of $\mathbf{P^4}H^+$. ICT character in protonated $\mathbf{P^4}$ is further agreed from the excited state optimized geometry of both protonated and deprotonated $\mathbf{P^4}$ molecules. In excited states the twisted angle between quinoline and phenyl groups is ~ 0°. But after protonation dihedral angle is increased to ~90° in the excited state. Dipole moment increases from 1.015 D to 3.427 D after protonation and this enhancement of the dipole moment supports ICT character in $\mathbf{P^4}H^+$.

6.3.12. TNP Sensor

Explosives are deliberated as the staple soil contaminants in war-affected areas. Therefore, the accurate and dependable detection of explosives is a key matter of international anxiety. TNP is an extensively used explosive because it shows superior explosive power. In addition, it is a strong allergen and is very harmful to human beings. Here, we have introduced AIEE property of $\mathbf{P^4}$ hydrosol as fluorescence 'turn off' sensor for sensing trace amount of TNP in aqueous medium.

To investigate the mode of interaction in **P**^{4} with TNP, we have carried out UV-Vis absorption studies of the **P**^{4} hydrosol in the presence of TNP. A new broad peak at a longer wavelength region at ~ 370 nm (***Fig. 6.10a***) is observed. The broad red shifted band at 370 nm steadily becomes prominent with the increased concentration of TNP for a fixed amount of **P**^{4} hydrosol. Strong electron deficient molecule, TNP can easily be attracted towards surface bound **P**^{4} within the hydrosol to form ground state complex and the red shifted (~ 370 nm) absorption band is the charge transfer band [384] between **P**^{4} and TNP. But the addition of other nitroaromatic compounds to **P**^{4} hydrosol does not show any change in the absorption spectrum due to their less electron deficient character to form charge transfer complex.

Fluorescence emission spectrum of **P**^{4} hydrosol (***Fig. 6.10b***) exhibits an intense emission peak at 359 nm. Fluorescence intensity is effectively quenched upon addition of TNP. Upon gradual addition of TNP to **P**^{4} hydrosol, the emission intensity decreases, but the PL spectral position remains unchanged. On the other hand, the other relevant competing nitroaromatics; 4-nitrophenol (NP), 2, 4-dinitrophenol (DNP), 4-nitro aniline (NA), 2, 4-dinitro toluene (DNT), dinitro benzene (DNB) have no remarkable quenching effect on the fluorescence spectra. This clearly demonstrates that strong ground state complexation between more electron deficient TNP and electron rich **P**^{4} causes fluorescence quenching of hydrosol. The plot of I_0/I versus concentration of TNP shows an upward curvature instead of a linear relationship (inset of ***Fig. 6.10c***), indicating that quenching efficiency increases with increasing concentration of the quencher and may be termed as the super amplified quenching effect [385,386]. Here the surface bound **P**^{4} within the aggregated **P**^{4} hydrosol act as active site for " turn off " fluorescence in presence of TNP. Since the number of such active sites is more than one for a given aggregated particle, this type of quenching shows deviation from Stern-Volmer plot.

The equation $I_0/I = 0.359e^{7.31405[TNP]}$ is obtained by fitting the concave curve of ***Fig. 6.10c***. The non-linear nature of the plot (***Fig. 6.10c***) suggests that either both static and dynamic quenching of PL intensity take place in presence of quencher TNP. This obscurity is resolved by measuring the fluorescence lifetime of **P**^{4} hydrosol in the presence and absence of TNP. Our measured fluorescence decay curves of **P**^{4} hydrosol both in the presence (42 ps) and absence of TNP (39 ps) are fitted with single-exponential decay and the fitted components are similar for both the cases (***Fig. 6.10d***). This unchanged fluorescence lifetime of **P**^{4} hydrosol in the presence of TNP indicates that the fluorescence quenching takes place through ground state complexation i.e. through the static quenching mechanism. At much lower concentration of TNP (inset of ***Fig. 6.10c***) a linear Stern-Volmer plot is obtained with a

quenching constant value of 7.8 × 10^4 M^{-1}. Fluorescence quenching study of **P^4** hydrosol in presence of other nitro aromatic compounds (TNP, NP, DNP, NA, DNT, DNB) are shown in ***Fig. 6.11a***. It is observed that the quenching efficiency of TNP is much higher than the other nitro aromatics (***Fig. 6.13*** & ***6.14*** and ***Table 6.1*** & ***Table 6.2***). Our measured **P^4** emission quenching efficiency (%) by different nitroaromatics (***Fig. 6.11b***) show that TNP (80%) is the strongest and then followed by NP(34%), DNP(15%), NA(12%), DNT(5%) and DNB(3%). We have carried out the anti-interference experiment to illustrate the selective sensing property of **P^4** hydrosol towards TNP. A bar diagram viewing fluorescence quenching of **P^4** hydrosol by TNP in presence of other nitroaromatics is shown in ***Fig. 6.12***. We further measured the limit of detection of TNP using 3σ method and the detection limit is found to be 0.43 μM.

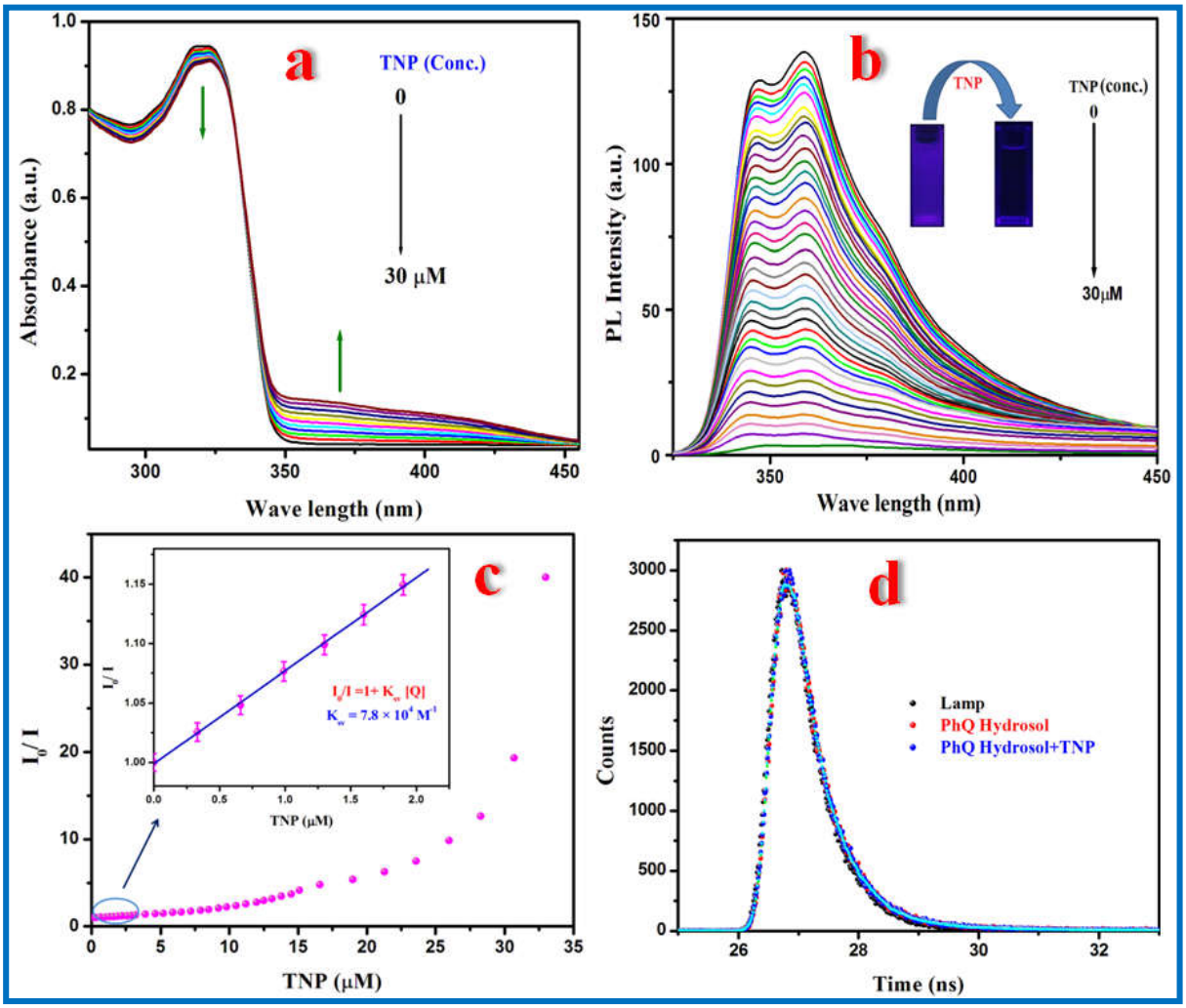

Fig. 6.10: (a) UV-Vis spectra and (b) Fluorescence spectra of **P^4** hydrosol (90 μM **P^4**) upon gradual addition of TNP (0-30 μM). λex: 315 nm. (c) Plot of I_0 /I versus concentration of TNP [TNP], added to **P^4** hydrosol. Inset: Stern-Volmer curve with Error Bars of fluorescence quenching in presence of different amount of TNP (d) Time resolved fluorescence decay curve of **P^4** hydrosol in absence and presence of TNP. λex: 291 nm & λem: 346 nm.

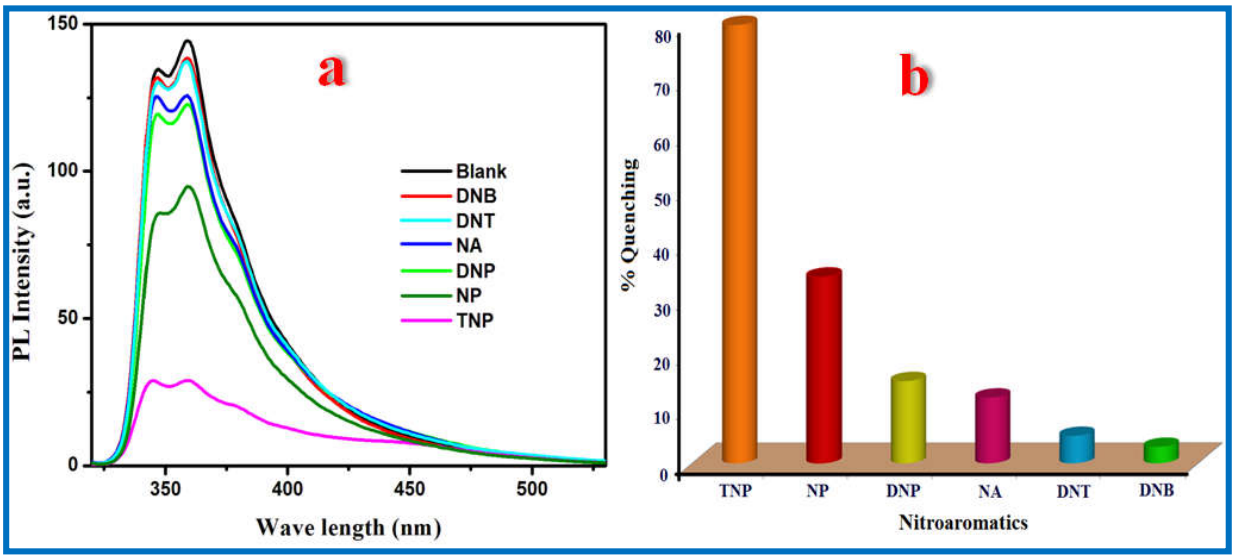

Fig. 6.11: a) Fluorescence emission spectra of P^4 hydrosol (90 µM) in presence of a fixed concentration (14.3µM) of different nitro-derivatives. (b) Bar diagram of fluorescence intensity of P^4 hydrosol (90 µM) after the addition of fixed concentration (14.3µM) of various nitro-aromatics.

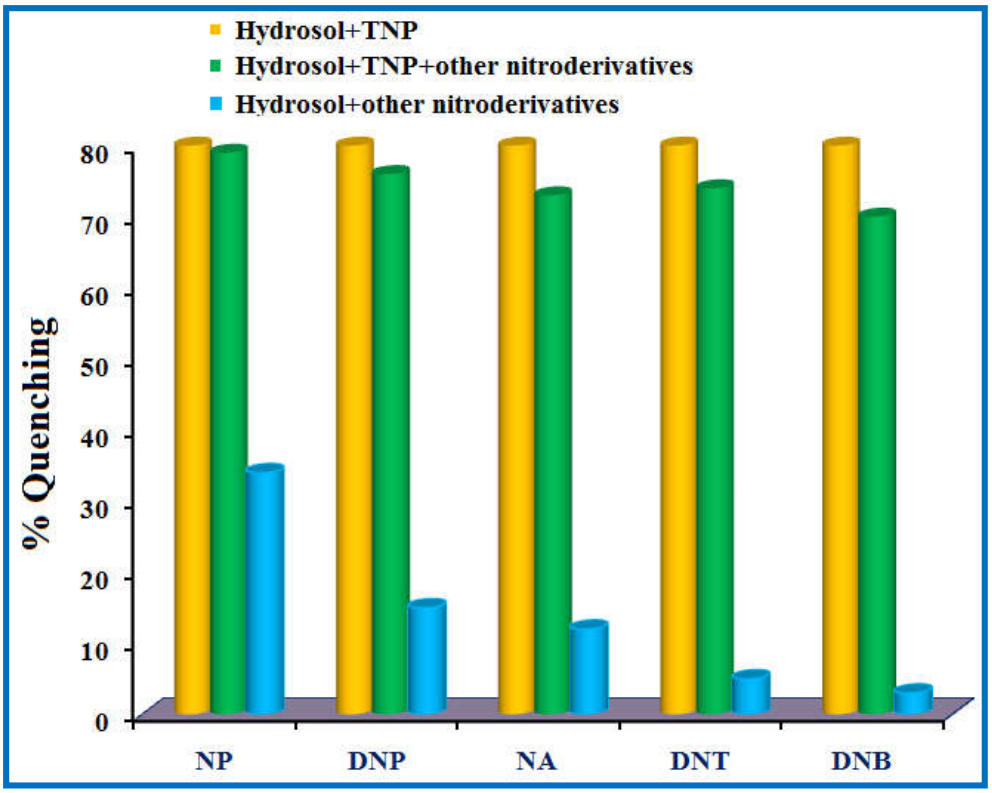

Fig. 6.12: Anti-interference experiment study of P^4 hydrosol

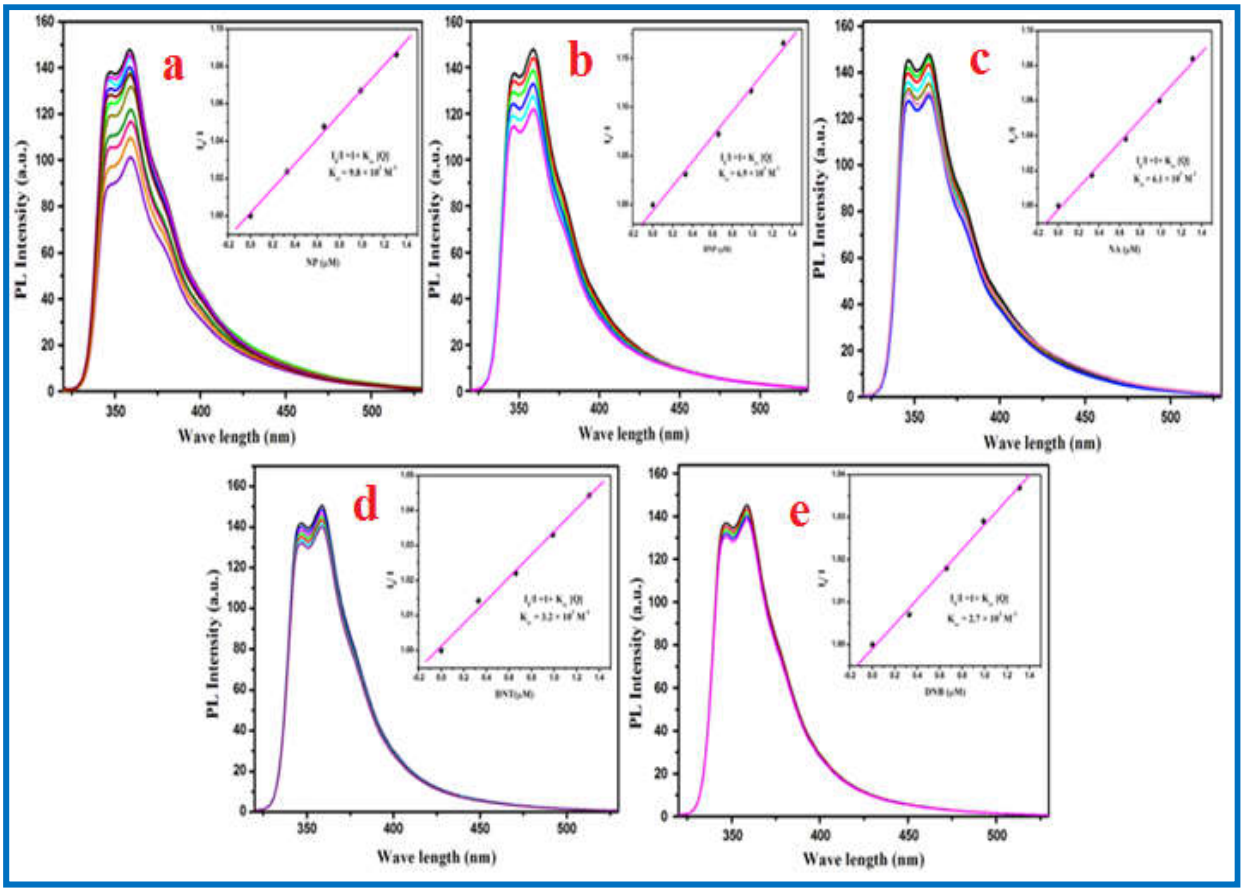

Fig. 6.13: Fluorescence Quenching of **P**[4] hydrosol in presence of (a) 4-Nitro-phenol (NP), (b) 2,4-dinitro-phenol (DNP), (c) 4-Nitroaniline (NA), (d) Dinitro-tolune (DNT), (e) Dinitro-benzene (DNB).

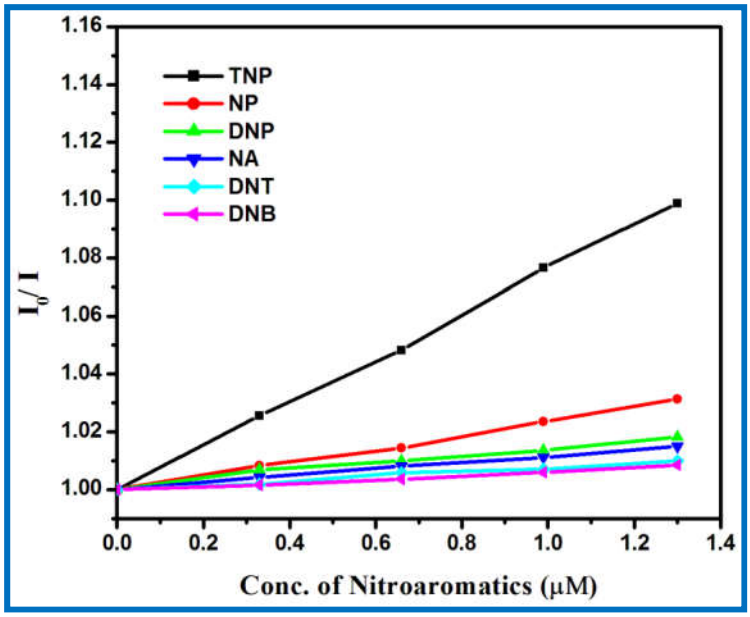

Fig. 6.14: Comparison of Stern-Volmer plot of different nitroaromatics.

Table 6.1: Stern-Volmer quenching constant (K_{SV} M^{-1}) for different nitroaromatics

Nitroaromatics	R	K_{SV} (M^{-1})
TNP	0.9930	7.8×10^4
NP	0.9981	9.8×10^3
DNP	0.9995	6.9×10^3
NA	0.9967	6.1×10^3
DNT	0.9975	3.2×10^3
DNB	0.9983	2.7×10^3

Table 6.2: A comparative study of our work with the other reported works in the literature with reference to K_{SV}, Detection limit and Anti interference study.

References	K_{SV} (M^{-1})	Detection limit	Anti interference
Anal. Methods, 2013,5,6228-6233	0.33	1 µM	-
Dalton Trans. 2013,42,12403-12409	-	4.5×10^{-7} M	-
ACS Appl. Mater. Interfaces 2013, 5, 672−679	1.55×10^4	3.5×10^{-7} M	-
RSC Adv., 2016, 6, 37929-37932	-	2.4×10^{-7} M	-
J. Mol. Liq. 224, 2016, 255–264	6.02×10^3	2.98×10^{-6} M	-
J. Photo Chem. & Photo Biology A. 2011,217,356-362	5.1×10^4	1×10^{-8} M	-
Org. Lett. 2012,14,3112-3115	6.9×10^4	500 ppb	-
J.Mater.Chem.A,2013, 1,8745-8752	3.4×10^4	8×10^{-8} M	-
Chem.commun.,2013, 49,4764	-	70 nM	-
J.Org. Chem., 2013,78,1306-1310	3.3×10^4	354 ppb	-
J. Mater. Chem.,2012,22,11574	3.04×10^4	2.38×10^{-8} M	-
Our present study	7.8×10^4	4.3×10^{-7} M	Yes

6.4. Conclusion

In this work, we have introduced a low dimensional aggregated hydrosol from the 2-phenyl quinoline (**P^4**) that possesses incredible AIEE properties. It exhibits very weak fluorescence in THF solution. Interestingly, the fluorescence intensity is increased enormously by the addition of 90% volume fraction of water. This increased PL intensity is due to restriction of intramolecular rotation and large amplitude vibrational modes of **P^4** in its aggregated state. The origin of fluorescence enhancement and morphology of the **P^4** aggregates have been addressed in the article. Microstructures of **P^4** with various morphologies have been synthesized using SDS as soft template. Morphologies of the particles were characterized using optical and scanning electron microscopy (SEM). Photophysical properties of aggregated **P^4** hydrosol were studied using UV–Vis absorption, steady state and time resolved fluorescence spectroscopy. Computation of HOMO, LUMO electron densities of **P^4** reveals intramolecular charge-transfer between phenyl and quinoline group taking place upon photoexcitation. Ratiometric fluorescence emission of **P^4** luminogen in presence of acid and base has been demonstrated as pH sensor for acidic and basic medium. The turn off fluorescence sensing property of aggregated **P^4** hydrosol is used for the selective detection of trace amounts of TNP with strong quenching constant (Ksv), 7.8 x10^4 M^{-1}. It is further explained with the help of both steady state and time resolved emission study that the fluorescence quenching of **P^4** hydrosol in presence of TNP takes place through static quenching mechanism.